Comparison of Raman Lidar Observations of Water Vapor with COSMO-DE Forecasts during COPS 2007

Christian Herold, Dietrich Althausen, Detlef Müller, Matthias Tesche, Patric Seifert, Ronny Engelmann, Cyrille Flamant, Rohini Bhawar, Paolo Di Girolamo

Comparison of Raman Lidar Observations of Water Vapor with COSMO-DE Forecasts during COPS 2007

CHRISTIAN HEROLD,*,& DIETRICH ALTHAUSEN,* DETLEF MÜLLER,*,+ MATTHIAS TESCHE,* PATRIC SEIFERT,* RONNY ENGELMANN,* CYRILLE FLAMANT,# ROHINI BHAWAR,@ AND PAOLO DI GIROLAMO@

* *Leibniz Institute for Tropospheric Research, Leipzig, Germany*
+ *Gwangju Institute of Science and Technology, Gwangju, South Korea*
# *Laboratoire Atmosphères, Milieux, Observations Spatiales, CNRS-UPMC-UVSQ, Paris, France*
@ *Dipartimento di Ingegneria e Fisica dell'Ambiente, Università degli Studi della Basilicata, Potenza, Italy*

(Manuscript received 4 June 2010, in final form 23 March 2011)

ABSTRACT

Water vapor measurements with the multiwavelength Raman lidar Backscatter Extinction Lidar-Ratio Temperature Humidity Profiling Apparatus (BERTHA) were performed during the Convective and Orographically-induced Precipitation Study (COPS) in the Black Forest, Germany, from June to August 2007. For quality assurance, profiles of the water vapor mixing ratio measured with BERTHA are compared to simultaneous measurements of a radiosonde and an airborne differential absorption lidar (DIAL) on 31 July 2007. The differences from the radiosonde observations are found to be on average 1.5% and 2.5% in the residual layer and in the free troposphere, respectively. During the two overflights at 1937 and 2018 UTC, the differences from the DIAL results are −2.2% and −3.7% in the residual layer and 2.1% and −2.6% in the free troposphere. After this performance check, short-range forecasts from the German Meteorological Service's (Deutscher Wetterdienst, DWD) version of the Consortium for Small-Scale Modeling (COSMO-DE) model are compared to the BERTHA measurements for two case studies. Generally, it is found that water vapor mixing ratios from short-range forecasts are on average 7.9% drier than the values measured in the residual layer. In the free troposphere, modeled values are 9.7% drier than the measurements.

1. Introduction

The Convective and Orographically-induced Precipitation Study (COPS) was an international field campaign incorporated within the framework of the German Research Foundation's (DFG) priority program Quantitative Precipitation Forecast (Wulfmeyer et al. 2008). The experiment took place in southwestern Germany and eastern France from June to August 2007. The aim was to improve quantitative precipitation forecasts over complex terrain by employing measurements of the atmospheric state (Kottmeier et al. 2008; Wulfmeyer et al. 2011). For this purpose, model outputs of water vapor profiles are compared with measured profiles.

Several water vapor measurement systems were deployed during COPS, allowing for a comparison of water vapor profiles measured with different techniques (Bhawar et al. 2011). One of the supersites of COPS was located in the Murg valley (Black Forest, 48°32′23″N, 8°23′50″E) at a height of 511 m MSL. At this supersite the Atmospheric Radiation Measurement (ARM) program of the U.S. Department of Energy deployed its mobile facility from 2 April to 31 December 2007 (information online at www.arm.gov/sites/amf/fkb/). During COPS, radiosondes were launched four times a day at this supersite.

The Leibniz Institute for Tropospheric Research (IfT) participated in COPS with the multiwavelength Raman lidar Backscatter Extinction Lidar-Ratio Temperature Humidity Profiling Apparatus (BERTHA). The system was placed right next to the ARM site. BERTHA simultaneously emits laser pulses at six wavelengths and

& Current affiliation: German Meteorological Service, Offenbach, Germany.

Corresponding author address: Dietrich Althausen, Leibniz Institute for Tropospheric Research, Permoserstr. 15, Leipzig D-04103, Germany.
E-mail: dietrich@tropos.de

DOI: 10.1175/2011WAF2222448.1

measures elastically and inelastically backscattered light in 14 channels. Details of the system are described by Althausen et al. (2000), Arshinov et al. (2005), and Tesche et al. (2009). In section 2 the applied water vapor measurement technique and the data retrieval scheme are presented. Comparisons of water vapor profiles measured with BERTHA and other systems are given in section 3. A discussion of measured and modeled water vapor profiles can be found in section 4. A short summary completes this contribution.

2. Water vapor measurements with BERTHA

The Raman lidar technique for atmospheric water vapor measurements was developed and first investigated by Melfi et al. (1969), Cooney (1970), and Melfi (1972). A review of the basics and recent realizations of Raman lidar systems for water vapor measurements is given by Wandinger (2005) and the references therein.

BERTHA (Althausen et al. 2000) has been developed for simultaneous measurements of aerosol, water vapor, and temperature profiles. The parts of BERTHA belonging to the water vapor measurements are similar to the realizations described in Wandinger (2005). Laser pulses at a wavelength of 355 nm are transmitted into the atmosphere. Part of this radiation is Raman shifted and backscattered by atmospheric water vapor and nitrogen molecules at the wavelengths of 407 and 386 nm, respectively. In the receiver of BERTHA the backscattered light is separated by dichroic beam splitters into different receiver channels. Neutral density filters are used in each channel to avoid saturation of the respective detector. Interference filters in front of the detectors are utilized to select light of the desired wavelength. For the water vapor measurements, an interference filter with a full width at half maximum (FWHM) of 0.25 nm and a maximum transmission at 407.475 nm is applied. For molecular nitrogen Raman backscatter measurements, an interference filter with an FWHM of 2.8 nm and a maximum transmission at 386.3 nm is implemented. Photomultiplier tubes are used for the time-dependent detection of backscattered light. For this study the 400-nm channel (see Althausen et al. 2000) is equipped with the 407-nm interference filter for water vapor measurements.

The water vapor mixing ratio $m_{H_2O}(z)$ at the height z is obtained from the quotient of the two signals $P_{\lambda_{H_2O}}$ and $P_{\lambda_{N_2}}$ multiplied by a calibration constant C_{H_2O} and the height-dependent transmission ratio of the atmosphere:

$$m_{H_2O}(z) = C_{H_2O}\frac{P_{\lambda_{H_2O}}}{P_{\lambda_{N_2}}}\frac{\exp\left[-\int_0^z \alpha_{\lambda_{N_2}}(\zeta)\,d\zeta\right]}{\exp\left[-\int_0^z \alpha_{\lambda_{H_2O}}(\zeta)\,d\zeta\right]}. \quad (1)$$

Here, $\alpha_{\lambda_i}(\zeta)$ describes the extinction caused by molecules and particles at the wavelength λ_i. The different molecular extinctions at the wavelengths of 407 and 386 nm, respectively, are described in Whiteman (2003) and were taken into account. The wavelength dependence of the particle extinction coefficient can be expressed by the following equation:

$$\frac{\alpha_{386}^{\text{par}}}{\alpha_{407}^{\text{par}}} = \left(\frac{407}{386}\right)^k. \quad (2)$$

For the presented study the Ångström exponent k of the particle extinction coefficient was not available. To quantify the effects of particle scattering, the height-dependent transmission ratio of the atmosphere, $\exp[-\int_0^z \alpha_{\lambda_{N_2}}(\zeta)\,d\zeta]/\exp[-\int_0^z \alpha_{\lambda_{H_2O}}(\zeta)\,d\zeta]$, was calculated. For this, an Ångström exponent of 1.5 and an aerosol optical thickness (AOT) of 0.4 were assumed at the wavelength of 396.5 nm for the residual layer with a top height of 2 km above ground level (AGL). Above the residual layer, an AOT of 0.02 was estimated to represent the conditions in the free troposphere. The AOT for the residual layer is twice as much as typical values for measurements during COPS. Figures 1a and 1b show vertical profiles of the calculated molecular and particle extinction, respectively. The resulting influence on the transmission ratio is depicted in Fig. 1c. The effect of particle scattering on the signal ratio was found to be less than 5% (Fig. 1c) even for these high AOTs. This effect gets reduced due to the calibration with radiosonde data. If particle extinction is neglected, a slightly different calibration constant, C_{H_2O}, is obtained. In the case of 31 July 2007, the calibration constant C_{H_2O} is 58.5 g kg^{-1}. If the particle extinction is taken into account, the calibration constant changes to 59.3 g kg^{-1}, which results in a maximum bias of 0.08 g kg^{-1} and an average bias of 0.02 g kg^{-1}. This deviation is well below the statistical errors of the mixing ratio measurements with BERTHA. Hence, the differential particle extinction was neglected in this study (see also Mattis et al. 2002).

An additional correction is performed to account for the temperature dependence of the water vapor Raman spectrum portion that is selected by the interference filter (Whiteman 2003). The temperature profile of the radiosonde is used for this correction.

The calibration constant has to be determined for each night measurement during COPS, because it strongly depends on the setup of the receiver (i.e., choice of neutral density filters).

Vaisala RS92 radiosondes were used for lidar calibration. The radiosonde station belonged to the ARM's

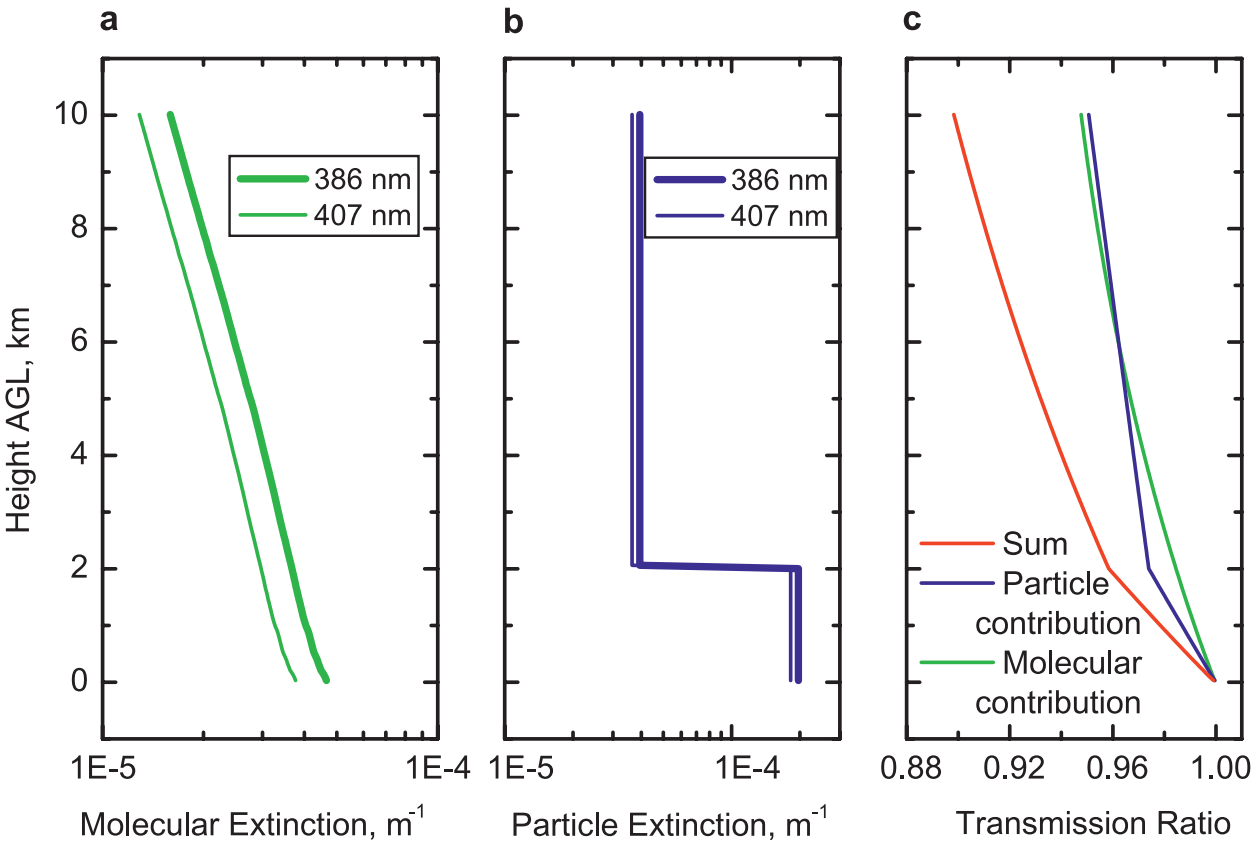

FIG. 1. (a) Calculated profile of the molecular extinction coefficient using a ground pressure of 1013 hPa and a ground temperature of 288 K (after Elterman 1968; Teillet 1990; Buchholz 1995; Whiteman 2003). (b) Calculated profile of the particle extinction coefficient (for details see text). (c) Transmission ratio considering the molecular contribution (green) and the particle contribution (blue), and considering both contributions (red).

mobile facility and was located about 15 m away from the lidar. There are several systematic errors of the radiosondes that are discussed by Vömel et al. (2007) and Miloshevich et al. (2009). Because no error bars are shown for radiosonde profiles in our study, a brief discussion is given. Regarding the error of the ground check, the ARM facility is cited as maintaining "good operational ground check procedures," which minimizes this error (Miloshevich et al. 2009). The time-lag error becomes noticeable above 14 km in the study by Vömel et al. (2007). Since only radiosonde profile data below 5-km height are used for the determination of the calibration constant, this error can be neglected in this study. The radiation error of the radiosondes has to be taken into account at low solar zenith angles ($\leq 30°$). This error can also be neglected in our study, because most of the time we used radiosondes launched during the nighttime. Only the radiosonde used for calibration on 5 August 2007 was launched before nightfall (at 1800 UTC). However, this sonde was launched at very large solar zenith angles.

For the data analysis, lidar data were averaged over 1 h. Then, the differential molecular extinction and the interference filter transmission were corrected. Due to the drift off of the radiosonde, only height ranges that showed similar vertical structures were used for the determination of the calibration constant. Usually, data between 1- and 5-km heights were used for the lidar calibration. A linear regression resulted in the calibration constant C_{H_2O} and its error.

In addition to these systematic errors of the lidar measurement, statistical errors had to be taken into account. The statistical errors of the Raman lidar measurements are caused by the statistics of the detected Raman-shifted photons and of the detected sky background photons. The total error of the water vapor measurement was determined by applying the law of error propagation (Mattis et al. 2002; Di Girolamo et al. 2009). Errors caused by the corrections of differential molecular transmission and of filter transmission dependence on water vapor temperature were neglected because these errors were found to be small compared to

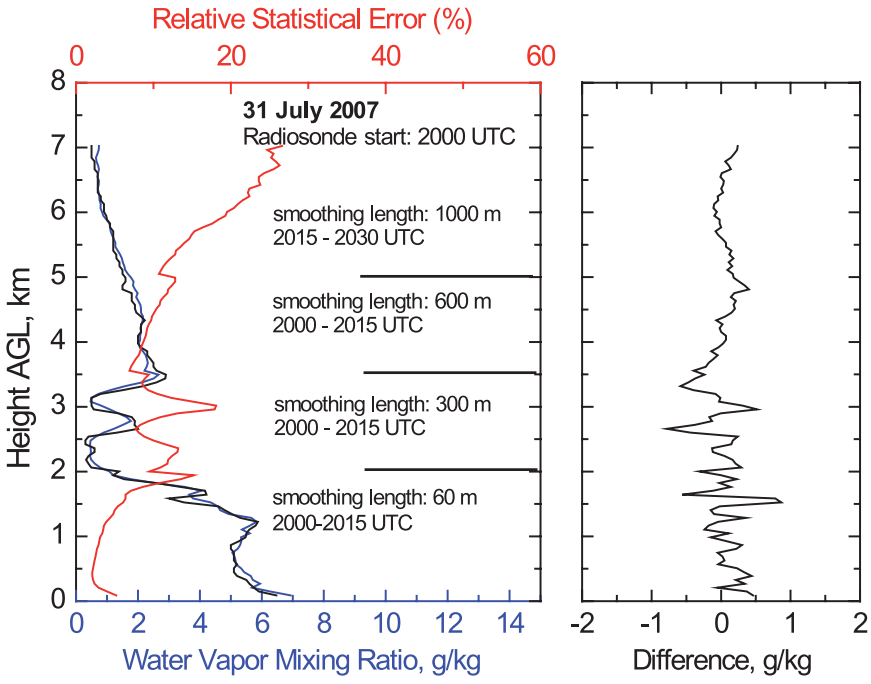

FIG. 2. (left) Comparison of the water vapor mixing ratio measured with lidar (blue) and radiosonde (black) at 2000 UTC 31 Jul 2007. The calibration constant C_{H_2O} was determined using the radiosonde launched at 2330 UTC 31 Jul 2007. The red line shows the relative statistical error of the lidar measurement. Black horizontal lines mark the different measurement times and the respective smoothing lengths. (right) The difference between lidar and radiosonde measurements.

the statistical errors and to the error of the calibration constant.

3. Comparisons of water vapor measurements

a. Comparison of BERTHA measurements with radiosonde data

On 31 July 2007 an additional radiosonde was launched at 2000 UTC. The neutral density filters were not changed between this evening radiosonde and the standard nighttime radiosonde at 2300 UTC. This allows for an investigation of the stability of the lidar calibration during the measurement. Figure 2 shows the comparison of water vapor mixing ratio profiles measured with BERTHA and radiosonde at 2000 UTC 31 July 2007. The calibration constant is determined using the radiosonde from 2300 UTC 31 July 2007. The lidar observation is averaged at 15-min intervals according to the time and height of the radiosonde during its ascent. Thus, the time shift between radiosonde and lidar measurements is minimized. The time intervals and the applied vertical smoothing lengths of the lidar data are indicated in Fig. 2.

The difference between the results of the lidar and radiosonde measurements is well below 1 g kg^{-1}. The mean differences between the lidar and the radiosonde data are 0.11 ± 0.30 g kg^{-1} (1.5 ± 8.6%) within the residual layer and 0.01 ± 0.21 g kg^{-1} (2.5 ± 19.2%) in the free troposphere.

The relative statistical error affecting the lidar measurements is smaller than 10% up to 1.8-km height AGL. By varying the height-dependent vertical smoothing window, the relative statistical error is kept below 20% up to about 6-km height AGL.

The differences between the lidar and the radiosonde may be associated with the radiosonde drift. However, this comparison of BERTHA measurements with a radiosonde profile shows the stability of the calibration constant for the lidar retrieval.

b. Comparison of BERTHA and the DIAL LEANDRE 2

A Raman lidar directly measures the water vapor mixing ratio. In contrast, the differential absorption lidar (DIAL) method determines the absolute humidity. The mixing ratio is then calculated by using the temperature profile from the radiosonde. The DIAL system Lidar pour l'Etude des Interactions Aérosols Nuages Dynamique Rayonnement et du Cycle de l'Eau

(LEANDRE 2) was operated aboard the Safire Falcon 20 (Bruneau et al. 2001a,b).

Behrendt et al. (2007) reported an overall relative bias value for LEANDRE 2 of 9.3% during the International H_2O Project (IHOP_2002). This bias had been determined on the basis of a water vapor intercomparison effort involving all airborne water vapor lidar systems operational during this field campaign. However, during IHOP_2002, LEANDRE 2 was flown on board the Naval Research Laboratory's (NRL) P-3, while it was flown on the Falcon 20 during COPS. In between these two field efforts the LEANDRE 2 system had been upgraded significantly, thereby justifying a new intercomparison exercise that has been carried out within the framework of COPS (Bhawar et al. 2011). This intercomparison involved all airborne and ground-based water vapor lidar systems operational during COPS. Based on the available statistics of comparisons, benefiting from the fact that the LEANDRE 2 was able to be compared with all other lidar systems, and putting equal weight on the data reliability of each instrument, overall relative bias values for all lidar systems were determined. Overall, the moist bias for LEANDRE 2 was found to be 1.72%.

Comparisons are shown for 1937 and 2018 UTC 31 July 2007 in the left panels of Fig. 3. The statistical error affecting the Raman lidar measurements varies between 0.2 and 1.5 g kg^{-1}. The right panels in Fig. 3 show the differences between the profiles of the two systems. The measurement at 1937 UTC took place under twilight conditions, which prohibited a comparison above 3.5-km height. The difference is less than 1 g kg^{-1} at all heights. The difference between the two lidars is similar to the difference between the lidar and the radiosonde. At 1937 UTC, the mean differences are -0.11 ± 0.25 g kg^{-1} ($-2.2 \pm 4.7\%$) within the residual layer and 0.09 ± 0.51 g kg^{-1} ($2.1 \pm 35.7\%$) in the free troposphere. At 2018 UTC, mean differences of -0.18 ± 0.33 g kg^{-1} ($-3.7 \pm 6.5\%$) within the residual layer and -0.09 ± 0.34 g kg^{-1} ($-2.6 \pm 38.1\%$) in the free troposphere are found.

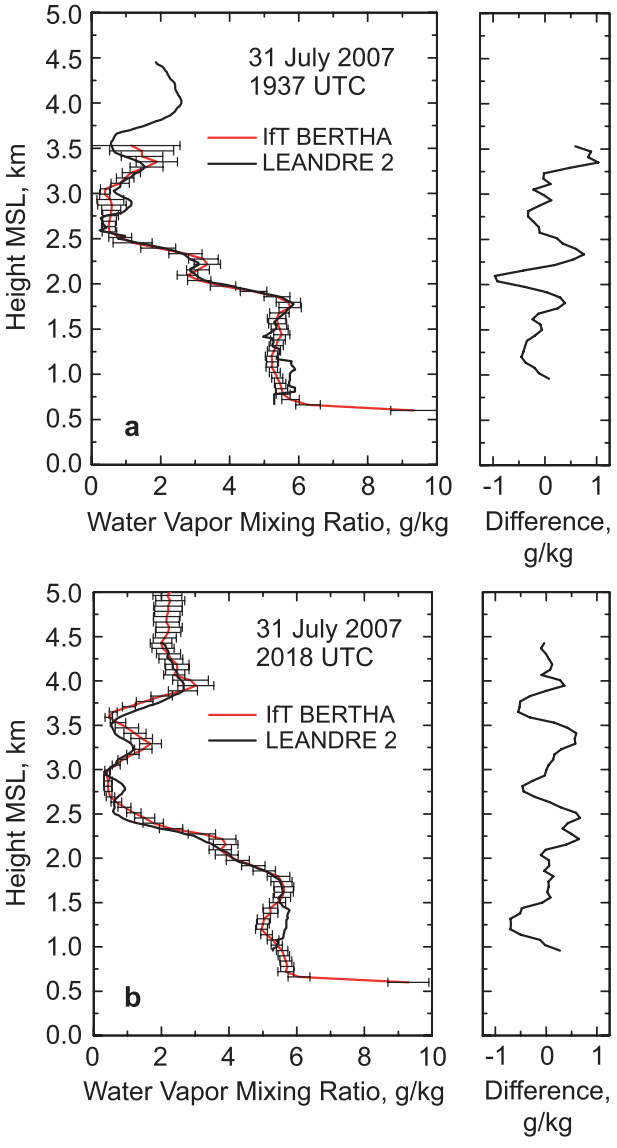

FIG. 3. (left) Comparison of water vapor profiles from BERTHA (red) and LEANDRE 2 aboard the Safire Falcon 20 (black) on 31 July 2007 at (a) 1937 UTC and (b) 2018 UTC. The height units are km MSL. (right) The difference in the measurements of BERTHA minus LEANDRE 2.

4. Comparison of measurements with results of the COSMO-DE model

The operational local model of the German Meteorological Service (Deutscher Wetterdienst, DWD) is based on the Consortium for Small-Scale Modeling (COSMO) model and is called COSMO-DE (Baldauf et al. 2011). The model delivers a 21-h forecast in steps of 1 h. The model is initiated 8 times a day. It covers an area of 1300×1200 km^2. The grid points are equidistant at 0.025° (≈2.8 km). This relatively high resolution of the COSMO-DE model allows for the coverage of small-scale phenomena such as convection or local orographic influences. The model comprises 50 layers. The lowermost layer is at the height of 10 m MSL and has a geometrical depth of 20 m. The height of the model layers is determined by an altitude-oriented hybrid coordinate, which causes an increase of the layer depth with height. The layers follow the model orography in the lower troposphere while they change to horizontal layers at higher altitudes. The uppermost layer is at 21 500 m MSL and has a geometrical depth of 1000 m. The model is operated with time steps of 30 s. The COSMO-DE

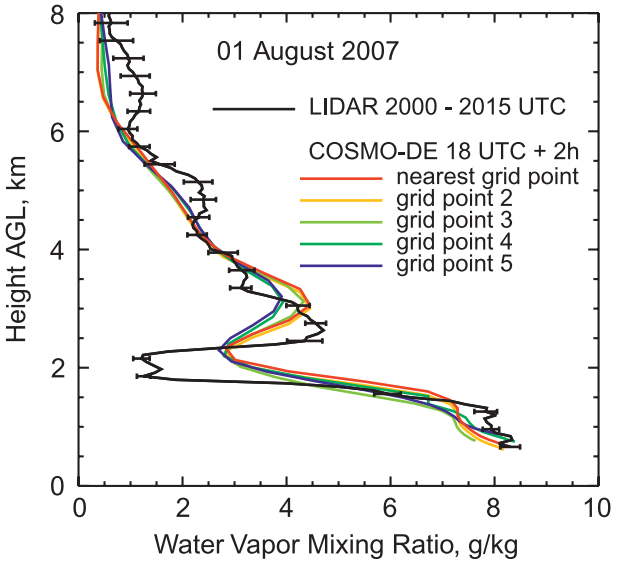

FIG. 4. Water vapor mixing ratio at 2000 UTC 1 Aug 2007 measured with lidar (black) and predicted from the COSMO-DE run started at 1800 UTC at the grid point next to the site (red) and at surrounding grid points each at a distance of about 10 km. These grid points are at even larger distances than those of neighboring grid points.

outputs of the COPS campaign are stored at the World Data Center for Climate and are accessible online (http://cera-www.dkrz.de/WDCC/ui/EntryList.jsp?acronym=dphase_lmk).

The grid point nearest to the COPS measurement site is located at 48°33′42″N and 8°24′22″E (670 m MSL), which is about 600 m away from the BERTHA instrument. The humidity values at grid points next to the nearest grid point differed by less than 0.2 g kg^{-1} each day. This is small compared to the measurement error of the lidar system.

Figure 4 shows the 2000 UTC forecast of vertical profiles of the water vapor mixing ratio from the 1800 UTC run of COSMO-DE on 1 August 2007. Profiles are shown at the nearest grid point and at the surrounding grid points at a distance of about 10 km. In all cases, the difference in the mixing ratio between the grid points is relatively small, even at larger distances and despite the differing orographic features. Given this small difference, only the profile at the nearest grid point is compared with the lidar measurement in the following.

For this comparison, lidar measurements of the water vapor mixing ratio are averaged at 15-min intervals. A height-dependent vertical moving average is used to reduce the relative statistical error that is caused by signal noise. The comparison is always performed with the forecasts of the 1800 UTC COSMO-DE run (by using the hourly forecasted output fields). The measured data are interpolated onto the COSMO-DE layer heights.

In the following two subsections, two case studies of the development of the water vapor mixing ratio are discussed. One case is the nighttime measurement on 31 July 2007. This case is characterized by high pressure conditions under the influence of dry polar air masses. In the second case, on the night of 2 August 2007, an approaching mesoscale convective system (MCS) caused the advection of humid layers into the prevailing stable air masses.

a. Case study from 31 July 2007

On 31 July 2007, an upper-level ridge with a corresponding surface high pressure system was identified over western Europe. The system was located between a long-wave trough from Scandinavia to eastern Europe and a trough over the eastern Atlantic. This surface high pressure system slowly moved eastward. The COPS region came under the influence of polar air masses between the western European high and the upper-level trough. The high pressure system caused a widespread subsidence in the COPS region.

In Fig. 5 the development of the water vapor mixing ratio on 31 July 2007 as measured by the lidar (panel a) and predicted by COSMO-DE (panel b, run at 1800 UTC) is shown. In the polar air mass the values of the water vapor mixing ratio were relatively low throughout the troposphere. Several humid layers are visible in the lidar profile. Below 1800-m height the detected layers are attributed to the nocturnal boundary layer and the residual layer (previous day's boundary layer), respectively. These layers are characterized by higher mixing ratios of about 5–6 g kg^{-1}. Above the residual layer (between 2- and 3-km heights), the mixing ratio showed values below 0.5 g kg^{-1}. The air masses above were slightly moister compared to this layer. The smoothing length and the time average of the lidar data were chosen to keep the relative statistical error of the water vapor mixing ratio measurements below 20% up to a height of 6.5 km AGL.

In Fig. 5c the difference between the lidar and the model data is presented. Red colors denote an overestimation of the water vapor mixing ratio by the model with respect to the measurements, whereas blue colors denote an underestimation. For the determination of the lidar profiles the same height-dependent vertical smoothing windows as indicated in Fig. 2 were used. The difference between the model predictions and the measurements is below 1 g kg^{-1} except for the height range between 1.3 and 3.3 km.

Figure 6 shows this comparison in more detail. COSMO-DE resolves the humid residual layer very well. Even the distinctive dry layer between the 1.8- and 3-km heights is predicted. The model does not forecast

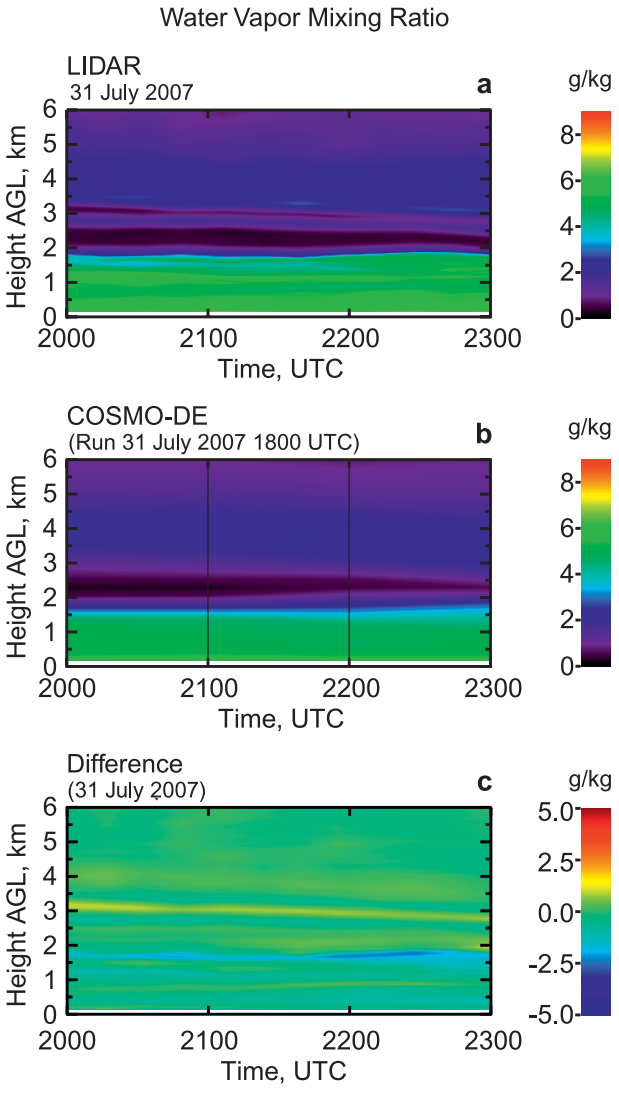

FIG. 5. (a) The measured water vapor mixing ratio (temporal smoothing of 15 min), (b) the predicted mixing ratio of the COSMO-DE run started at 1800 UTC (linearly interpolated between the outputs on the clock hours), and (c) the difference in the predicted minus measured mixing ratio for 31 Jul 2007.

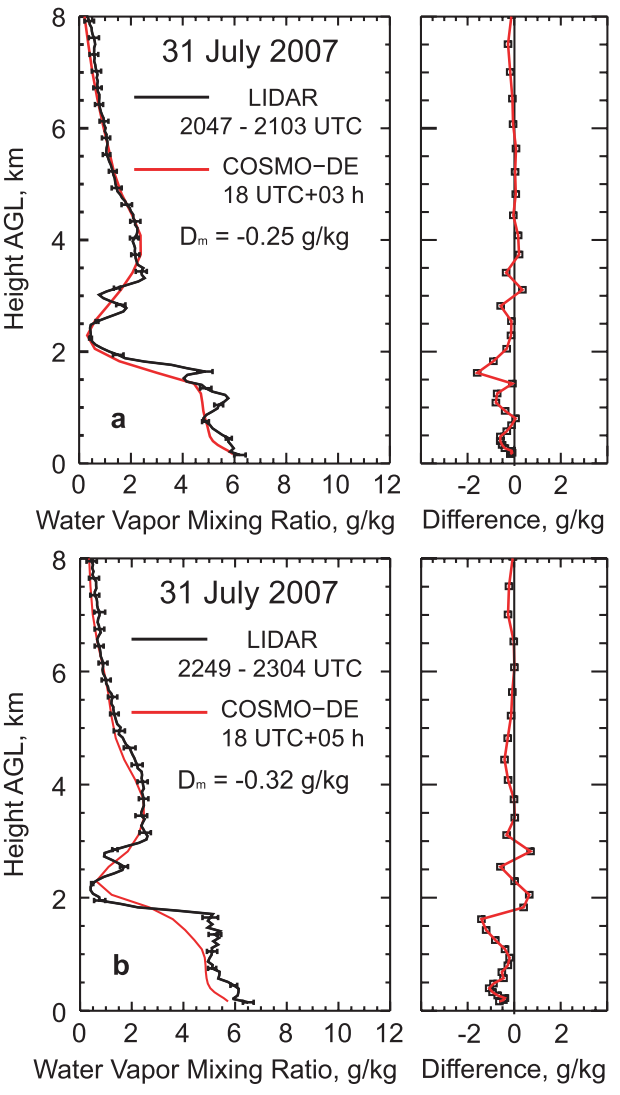

FIG. 6. (left) Vertical profiles of the water vapor mixing ratio measured with lidar (black) and predicted by the COSMO-DE run started at 1800 UTC 31 Jul 2007 (red). Here, D_m denotes the mean difference. (right) The differences between the profiles (COSMO-DE minus BERTHA).

the slightly humid layer between the 2.5- and 2.7-km heights, which was detected by the lidar. The largest difference occurs at the transition height between the residual layer and the overlying dry air layer. Differences of up to -2 g kg^{-1} are found. The lidar measured strong gradients in the water vapor concentration, which are not resolved by the model. In the free troposphere above 3-km height, the agreement between the model and the measurements is very good. The mean difference between the model forecast and the lidar measurements on this day is $-7.5\% \pm 13.3\%$ in the residual layer (top height of 1.82 km). For the free troposphere a mean difference of -6.3% is obtained. The standard deviation of 20.4% in the upper layers is still within the range of the relative statistical measurement error.

b. *Case study of the night of 1–2 August 2007*

On 2 August 2007 central Europe was under the influence of an upper-level ridge at the rear of a weakening trough that moved eastward. High pressure conditions were present at the surface. Another trough moved slowly from the eastern Atlantic toward western Europe. Ahead of this trough, warm air and differential vorticity were advected and triggered cyclogenesis along the eastern flank of the trough. This configuration formed a depression that strengthened over France.

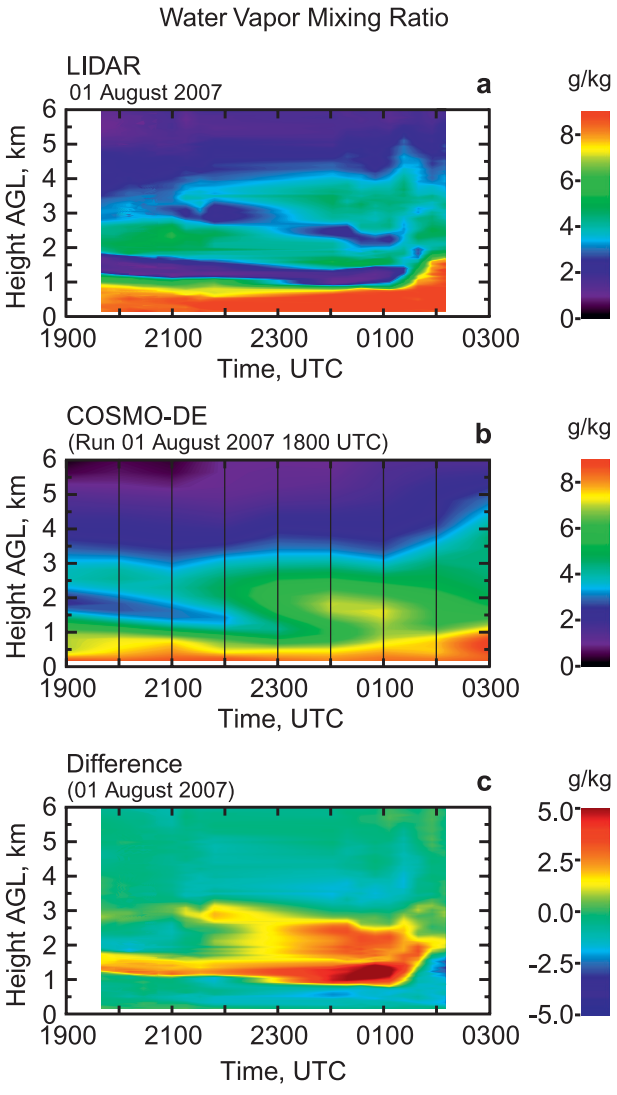

FIG. 7. (a) The measured water vapor mixing ratio (temporal smoothing of 15 min), (b) the predicted mixing ratio of the COSMO-DE run started at 1800 UTC 1 Aug 2007 (linearly interpolated between the outputs on the clock hours), and (c) the difference in the predicted minus measured mixing ratio for 1–2 Aug 2007.

In the unstable air mass over France, a surface convergence was formed and led to numerous thunderstorms, which developed into an MCS. This system was moving in a northeasterly direction and weakened during the night. The precipitation of the MCS reached the measurement site at around 0300 UTC.

As can be seen in Fig. 7, the layer from the ground up to a height of 1.1 km can be assigned to the nocturnal residual layer. A very dry layer was situated above the nocturnal residual layer. A back-trajectory analysis showed that this dry layer was caused by the subsidence of dry air masses from higher altitudes. Between 2- and 5-km heights, high aerosol backscatter values were measured (not shown). The corresponding air mass had passed the Sahara Desert. In this layer the mixing ratio reached values as large as 5 g kg^{-1}, which is a typical value for a Saharan air mass (Saïd et al. 2010; English et al. 1994). Later, a drier well-mixed layer pervaded this height range. After about 0130 UTC the humid layers were lifted due to the approaching outflow boundary of the MCS. The top of the residual layer was lifted by more than 2 km. The overlaying dry air layers were also lifted and mixed with the Saharan air mass.

Figure 8 shows four selected measured and forecasted vertical profiles of the water vapor mixing ratio, together with the differences between the two profiles for the night of 1–2 August 2007. The main vertical structures of the water vapor mixing ratio are covered by the COSMO-DE model, but significant differences occur. The minimum of the measured humidity profile in the 1–1.5-km height range was smaller at the beginning (see profiles at 2000–2015 and 2100–2115 UTC). This minimum was not even forecasted by COSMO-DE at later times (profiles at 0050–0105 and 0150–0205 UTC and in Fig. 7b after 2300 UTC). As a result, very large differences of up to 4 g kg^{-1} occur in this height range (see Fig. 7c). Measurements and predictions both show a subsidence of the dry layer between the 1- and 1.7-km heights. In the COSMO-DE run, the dry layer disappears almost completely due to the advection and mixing of humid air masses into the free troposphere. The lidar observed a different pattern of development for the vertical water vapor distribution. The dry layer persisted until the arrival of the MCS. This observation explains the deviations between the observations and the model at this height range. The advection of moister air masses in the free troposphere forecasted by COSMO-DE is also less dominant in the lidar observations. The dry layer between the 2- and 3-km heights (subsiding with time) was not predicted by the model. Also, the uplift of the moist layer at the end of the forecast period was not predicted correctly by COSMO-DE. The measurements during the night of 1–2 August 2007 showed a mean difference in the model values of −9.2% with a standard deviation of 12.5% in the residual layer and a mean difference of −11.5% with a standard deviation of 31.0% in the free troposphere between the 1.1- and 8-km heights. The standard deviation for the free troposphere is in the range of the measurement error.

c. *Statistical investigation*

The comparison with model predictions was performed for all available lidar measurements during the COPS campaign. Since the water vapor content in the

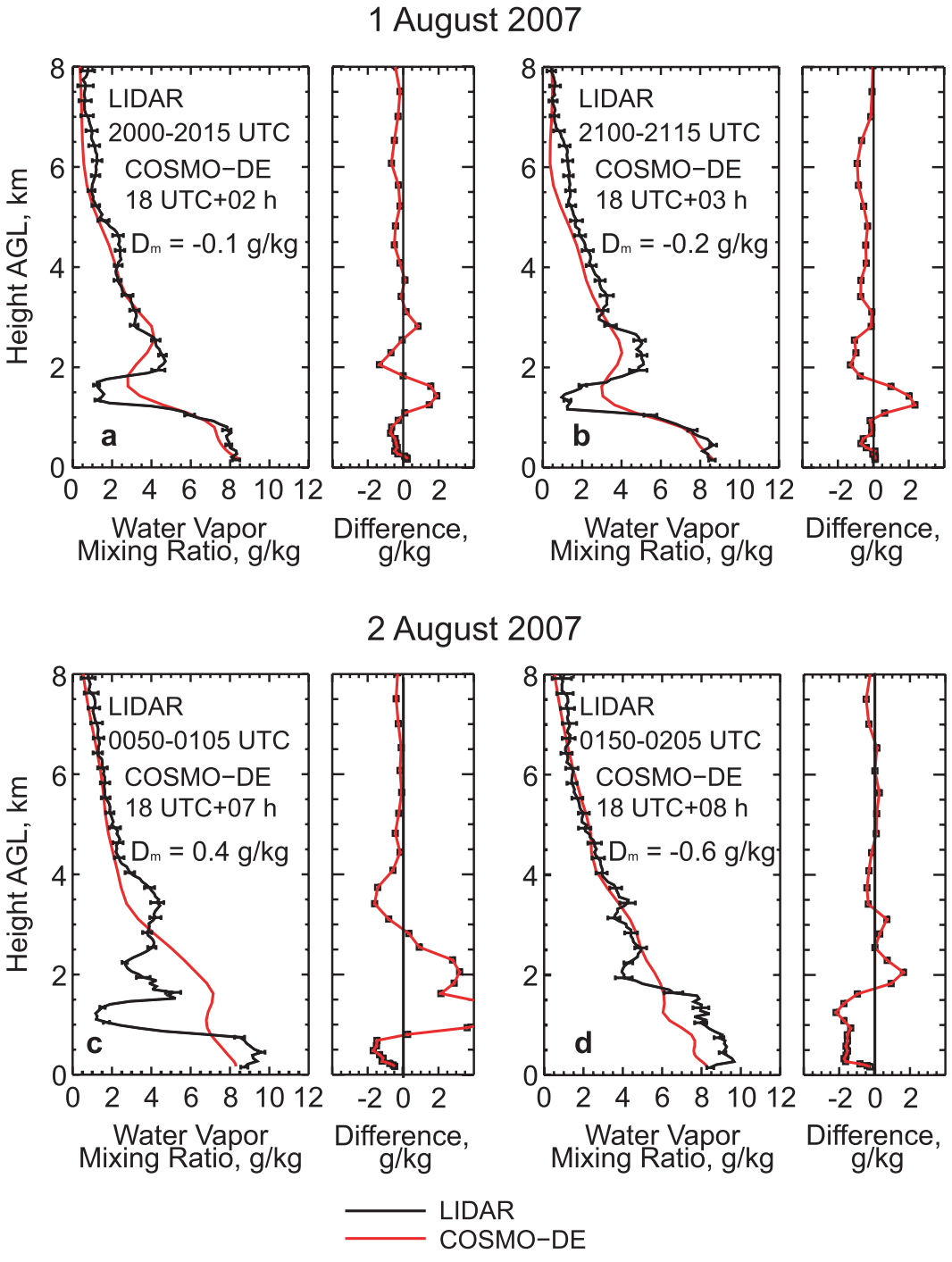

FIG. 8. Vertical profiles of the water vapor mixing ratio measured with lidar (black) and predicted by the COSMO-DE run started at 1800 UTC 1 Aug 2007 (red) for (top) 1 Aug 2007 and (bottom) 2 Aug 2007. (right) The differences in the profiles (COSMO-DE minus BERTHA).

residual layer usually is larger than in the free troposphere, comparisons were performed for the residual layer and the free troposphere, separately. The results are summarized in Table 1.

In the residual layer the values of the water vapor mixing ratio predicted by COSMO-DE were on average 7.9% lower than the measured values. In only one case (15 July 2007) did the model output predict values larger

TABLE 1. Mean differences between COSMO-DE forecasts of water vapor mixing ratio and the measured values (Diff) and corresponding standard deviations (Std dev). Values are shown for the residual layer (mean top height given as RLTOP) and the free troposphere up to 8-km height.

				Residual layer		Free troposphere	
Date	Time lidar (UTC)	Time COSMO-DE (UTC)	RLTOP (km)	Diff (%)	Std dev (%)	Diff (%)	Std dev (%)
30 Jun 2007	2300–0245	1800 + 5–1800 + 8	1.90	−3.1	19.8	−12.4	26.7
13 Jul 2007	2200	1800 + 4	1.45	−3.7	15.0	6.8	23.4
14 Jul 2007	2145–0400	1800 + 4–1800 + 10	2.10	−9.0	14.5	−6.3	31.2
15 Jul 2007	0000–0300	1800 + 6–1800 + 9	3.75	3.1	26.8	7.9	57.2
18 Jul 2007	2100–2300	1800 + 3–1800 + 5	4.00	−7.3	14.5	−9.3	24.0
25 Jul 2007	2200–0300	1800 + 4–1800 + 9	2.00	−13.5	17.4	1.2	73.4
26 Jul 2007	2000–2200	1800 + 2–1800 + 4	2.00	−6.6	16.5	−15.5	47.1
31 Jul 2007	2000–2300	1800 + 2–1800 + 5	1.82	−7.5	13.3	−6.3	20.4
1 Aug 2007	1940–0210	1800 + 2–1800 + 8	1.10	−9.2	12.5	−11.5	31.0
5 Aug 2007	2000–2100	1800 + 2–1800 + 3	1.50	−2.1	7.5	−84.2	101.7
12 Aug 2007	2100–2200	1800 + 3–1800 + 4	3.20	−5.9	12.2	6.5	26.4
15 Aug 2007	2100–2200	1800 + 3–1800 + 4	2.90	−22.2	23.4	—	—
23 Aug 2007	2100–2200	1800 + 3–1800 + 4	2.20	−13.9	15.3	0.6	20.4
24 Aug 2007	1900–2000	1800 + 1–1800 + 2	2.80	−7.0	9.8	−7.6	17.7
25 Aug 2007	2100–2200	1800 + 3–1800 + 4	2.80	−11.1	14.4	−6.5	52.9
Mean				−7.9	15.5	−9.7	39.5

than the measured ones, with a difference of +3.1%. To check whether the difference between measured and predicted values is significant, a one-sided *t* test was performed (Bronstein et al. 2001). The *t* test is a hypothesis test with Student's *t*-distributed test values. Based on the mean of a sample, this method proves whether the mean of a population is smaller than, equal to, or larger than a given value. It has to be assumed that the values are normally distributed and are not autocorrelated. An autocorrelation of the values cannot, however, be excluded with certainty. The *t* test showed that the values predicted by the model were significantly smaller than the values measured with lidar [$t(0.99, 14) = 2.624 < 5.17$]. The *t* test stresses that COSMO-DE systematically underestimates the humidity in the residual layer.

5. Summary

During the COPS campaign, water vapor profiles were measured with the IfT multiwavelength Raman-lidar BERTHA. Comparisons of BERTHA's results with radiosonde profiles and with profiles from the DIAL LEANDRE 2 aboard the French Safire Falcon 20 research aircraft on 31 July 2007 are presented. The comparison with the radiosonde data resulted in very small mean differences of 1.5% within the residual layer and of 2.5% in the free troposphere. The results of the comparisons between the ground-based lidar BERTHA and the airborne lidar LEANDRE 2 are in quite good agreement, with a 2%–3% difference. Both comparisons show the good performance and quality of the BERTHA system for water vapor measurements.

To verify the water vapor predictions of the COSMO-DE local model, all water vapor profiles from the COPS experiment measured with BERTHA were compared with the model output. Two examples are discussed in detail. A dry polar air mass under high pressure conditions was predominant on 31 July 2007, whereas on 1 August 2007 the measurements were performed before and during the approach of the outflow boundary of an aging MCS (i.e., before a convective event). The two cases discussed here indicate that the model represents the humidity distribution in a relatively steady atmosphere under high pressure conditions better than under cyclonic conditions before a strong convective event. A statistical analysis of the differences between model outputs and measurements showed that the COSMO-DE systematically underestimated the water vapor mixing ratio in the nocturnal residual layer by on average 8% and in the free troposphere by on average 10%. All water vapor profiles of the lidar BERTHA taken during the COPS period can be found on the COPS Web server (http://www.mad.zmaw.de/projects-at-md/cops-campaign/).

Acknowledgments. The COPS field campaign was supported by the DFG via Priority Programme 1167. The authors also thank Michael Denhard of the German Meteorological Service for providing the COSMO-DE outputs.

REFERENCES

Althausen, D., D. Müller, A. Ansmann, U. Wandinger, H. Hube, E. Clauder, and S. Zörner, 2000: Scanning 6-wavelength 11-channel aerosol lidar. *J. Atmos. Oceanic Technol.,* **17,** 1469–1482.

Arshinov, Y., S. Bobrovnikov, I. Serikov, A. Ansmann, U. Wandinger, D. Althausen, I. Mattis, and D. Müller, 2005: Daytime operation of a pure rotational Raman lidar by the use of a Fabry–Perot interferometer. *Appl. Opt.,* **44,** 3593–3603.

Baldauf, M., J. Förstner, S. Klink, T. Reinhardt, C. Schraff, A. Seifert, and K. Stephan, 2011: Short description of the convection resolving model COSMO-DE (LMK) and its databases on the data server of DWD. [Available online at http://www.dwd.de/bvbw/generator/DWDWWW/Content/Forschung/FE1/Veroeffentlichungen/Download/LMK__DBbeschr__1104__en,templateId=raw,property=publicationFile.pdf.]

Behrendt, A., and Coauthors, 2007: Intercomparison of water vapor data measured with lidar during IHOP_2002. Part II: Airborne-to-airborne systems. *J. Atmos. Oceanic Technol.,* **24,** 22–39.

Bhawar, R., and Coauthors, 2011: The water vapour intercomparison effort in the framework of the Convective and Orographically-Induced Precipitation Study: Airborne-to-ground-based and airborne-to-airborne lidar systems. *Quart. J. Roy. Meteor. Soc.,* **137,** 325–348, doi:10.1002/qj.697.

Bronstein, I. N., K. A. Semendjajew, G. Musiol, and H. Muehlig, 2001: *Taschenbuch der Mathematik*. Verlag, 1123 pp.

Bruneau, D., P. Quaglia, C. Flamant, M. Meissonnier, and J. Pelon, 2001a: The airborne lidar LEANDRE 2 for water vapor profiling in the troposphere. Part I: Description. *Appl. Opt.,* **40,** 3450–3461.

——, ——, ——, and J. Pelon, 2001b: The airborne lidar LEANDRE 2 for water vapor profiling in the troposphere. Part II: First results. *Appl. Opt.,* **40,** 3462–3475.

Buchholz, A., 1995: Rayleigh-scattering calculations for the terrestrial atmosphere. *Appl. Opt.,* **35,** 2765–2773.

Cooney, J., 1970: Comparisons of water vapor profiles obtained by radiosondes and laser backscatter. *J. Appl. Meteor.,* **10,** 301–308.

Di Girolamo, P., D. Summa, and R. Ferretti, 2009: Multiparameter Raman lidar measurements for the characterization of a dry stratospheric intrusion event. *J. Atmos. Oceanic Technol.,* **26,** 1742–1762.

Elterman, L., 1968: UV, visible, and IR attenuation for altitudes to 50 km. AVCLR-68-0153, U.S. Air Force Cambridge Research Laboratory, 56 pp.

English, S. J., C. Guillou, C. Prigent, and D. C. Jones, 1994: Aircraft measurements of water vapour continuum absorption at millimetre wavelengths. *Quart. J. Roy. Meteor. Soc.,* **120,** 603–625, doi:10.1002/qj.49712051706.

Kottmeier, C., and Coauthors, 2008: Mechanisms initiating deep convection over complex terrain during COPS. *Meteor Z.,* **17,** 931–948.

Mattis, I., and Coauthors, 2002: Relative-humidity profiling in the troposphere with a Raman lidar. *Appl. Opt.,* **41,** 6451–6462.

Melfi, S. H., 1972: Remote measurement of the atmosphere using Raman scattering. *Appl. Opt.,* **11,** 1605–1610.

——, J. D. J. Lawrence, and M. P. McCormick, 1969: Observation of Raman scattering by water vapor in the atmosphere. *Appl. Phys. Lett.,* **15,** 295–297.

Miloshevich, L. M., H. Vömel, D. N. Whiteman, and T. Leblanc, 2009: Accuracy assessment and correction of Vaisala RS92 radiosonde water vapor measurements. *J. Geophys. Res.,* **114,** D11305, doi:10.1029/2008JD011565.

Saïd, F., G. Canut, P. Durand, F. Lohou, and M. Lothon, 2010: Seasonal evolution of boundary-layer turbulence measured by aircraft during the AMMA 2006 Special Observation Period. *Quart. J. Roy. Meteor. Soc.,* **136** (S1), 47–65, doi:10.1002/qj.475.

Teillet, P. M., 1990: Rayleigh optical depth comparisons from various sources. *Appl. Opt.,* **29,** 1897–1900.

Tesche, M., and Coauthors, 2009: Vertical profiling of Saharan dust with Raman lidars and airborne HSRL in southern Morocco during SAMUM. *Tellus,* **61B,** 144–164.

Vömel, H., and Coauthors, 2007: Radiation dry bias of the Vaisala RS92 humidity sensor. *J. Atmos. Oceanic Technol.,* **24,** 953–963.

Wandinger, U., 2005: Raman lidar. *Lidar–Range-Resolved Optical Remote Sensing of the Atmosphere,* C. Weitkamp, Ed., Springer, 241–271.

Whiteman, D., 2003: Examination of the traditional Raman lidar technique. I. Evaluating the temperature-dependent lidar equation. *Appl. Opt.,* **42,** 2571–2592.

Wulfmeyer, V., and Coauthors, 2008: The Convective and Orographically induced Precipitation Study: A research and development project of the World Weather Research Program for improving quantitative precipitation forecasting in low-mountain regions. *Bull. Amer. Meteor. Soc.,* **89,** 1477–1486.

——, and Coauthors, 2011: The Convective and Orographically-Induced Precipitation Study (COPS): The scientific strategy, the field phase, and first highlights. *Quart. J. Roy. Meteor. Soc.,* **137,** 3–30, doi:10.1002/qj.752.